Research & Reviews: Journal of Material Sciences e-ISSN: 2321-6212

The Mechanical and Electronic Properties of Ternary Rare-Earth Hexaboride $La_xNd_{8-x}B_6$ (x=0,1,7,8) Materials

Cengiz Bozada*

Department of Metallurgical and Material Science Engineering, Gaziantep University, Gaziantep, Turkey

Research Article

Received: 21-Jan-2022, Manuscript No. JOMS-22-52044; **Editor assigned:** 24-Jan-2022, PreQC No. JOMS -22-52044(PQ); **Reviewed:** 04-Feb-2022, QC No. JOMS -22-52044; **Revised:** 06-Feb-2022, Manuscript No. JOMS -22-52044(R); **Published:** 13- Feb-2022, DOI: 10.4172/2321-6212.10.2.004.

***For Correspondence:**

Cengiz Bozada, Department of Metallurgical and Material Science Engineering, Gaziantep University, Gaziantep, Turkey

E-mail: b.ankara@yandex.com

Keywords: Rare-earth hexaboride; Lattice constant; PDOS; Charge density

ABSTRACT

We have carried out density functional theory to study the lattice constants and electronic properties of LaB_6, NdB_6, Nd-doped LaB_6, and La-doped NdB_6. The lattice constant, intra-octahedral bond, inter-octahedral boron bond, and positional parameter (z) were calculated for LaB_6, $La_7Nd_1B_6$, $La_1Nd_7B_6$, and NdB_6. Our results show that the doped Nd increases the lattice constant of $La_7Nd_1B_6$. Likewise, La-doping leads to an increase in the lattice constant of the $La_1Nd_7B_6$. The PDOSs of LaB_6, B of LaB_6, $La_7Nd_1B_6$, B of $La_7Nd_1B_6$, $La_1Nd_7B_6$, B of $La_1Nd_7B_6$, NdB_6, and B of NdB_6 were calculated. La d-electron bands cross the Fermi energy, showing classical conductor behaviour. The charge density results indicate that light and dark colours show high and low-intensity zones, respectively. $La_1Nd_7B_6$ has a low-density region and LaB_6 has a high-density region. The LaB_6 midpoint has strong charge density peaks. Weak peaks are also observed for $La_1Nd_7B_6$. Thus, ternary REB_6 has good potential for many applications. This article reports an investigation of the electronic features and structural parameters of binary and ternary hexaborides.

INTRODUCTION

Rare-Earth hexaborides (REB_6) are commonly used in various high-energy optical devices and field electron emitter systems because of their superior properties such as high chemical stability, high melting point, high mechanical strength, high brightness, low work function, low volatility, conductibility, small visual dimensions and long lifetimes [1]. REB_6 is commonly used as cathode material. REB_6 has a cubic CsCl-type structure with a space group of Pm-3m symmetry, in which a Rare-Earth (RE) ion occupies the Cs site; the B_6 octahedron is located on the Cl site. REB_6 compounds include LaB_6, CeB_6, PrB_6, NdB_6, PmB_6, SmB_6, EuB_6, GdB_6, TbB6, DyB_6, HoB_6, ErB_6, TmB_6, YbB_6, LuB6, ScB_6 and YB_6. LaB_6 has low volatility, CeB_6 indicates a typical dense Kondo behavior, PrB_6 shows high density, NdB_6 has low magnification, SmB_6 is a typical valence semiconductor and GdB_6 has the lowest work function among REB_6 compounds[2].

The electronic structures of the doped and binary REB_6 were calculated using Density Functional Theory (DFT). The position of the Fermi energy level and DOS were adjusted by doping with REB_6 to improve the electron emission

characteristics. The high-density d-orbital electrons play a crucial role in considerably decreasing the work function of REB_6 and contributing to the electronic states of electron emission near the Fermi level. This ensure excellent emission characteristics[3]. The Second-Order Elastic Constants (SOECs) and Third-Order Elastic Constants (TOECs) of LaB_6 and CeB_6 were studied by first-principles calculations. The effect of increased pressure on the elastic anisotropy, mechanical characteristics and structural stability of LaB_6 and CeB_6 has attracted considerable attention. When the pressure increases, the mechanical stability decreases and the ductility and anisotropy increase[4]. Lanthanum hexaboride (LaB_6) are superb thermionic and field electron emission cathode materials in the field of electron emission. LaB_6 has several applications in high-power electronics owing to its long lifetime and high luminosity. LaB_6 attracts attention by its low work function between 2.6 and 2.8 eV, its high melting point of 2715°C, and its stable chemical and physical characteristics. Compared to polycrystalline and single-crystal applications of LaB_6, it has better potential for single-crystal applications [5]. LaB_6 works well as a thermal-field emitter. It is easily degradable and stable in air. LaB_6 was reactive at 2715°C. LaB_6 is a violet-colored metal and its electron conductivity is approximately 1/5 that of copper [6]. Lu et al.[7] successfully fabricated LaB_6 nanocubes with an average dimension of 94.7 nm using a low-temperature molten salt technique at 800°C. LaB_6 nanocubes exhibited high Near-Infrared (NIR) adsorption. As mentioned in, LaB_6 nanocrystalline preparation routes include many synthesis routes such as the floating zone method, aluminum flux, molten salt, high-temperature reaction, Chemical Vapor Deposition (CVD), direct solid-phase reaction and carbothermal reduction [8]. It is because of its wonderful characteristics that LaB_6 is commonly used in some electrical devices, including free-electron laser, thermionic electron cathode, electron microscope, vacuum, and electron beam welder[9].

MATERIALS AND METHODS

Neodymium hexaboride (NdB_6) is black solid with good chemical stability, magnetic properties, electrical conductivity, and thermal conductivity characteristic. NdB_6 is insoluble in Hydrofluoric acid (HF) and hydrochloric acids (HCl). However, it can be dissolved in molten alkali, sulfuric acid (H_2SO_4) and nitric acid (HNO_3). In addition, it exhibits very high antioxidant capability[10]. NdB_6 crystallizes in a CsCl-type structure with a space group of Pm3m symmetry, where the Neodymium (Nd) occupies the Cs site and octahedral B_6 molecules are located at the Cl site. NdB_6 has a low work function (1.6 eV)[11]. NdB_6 are an efficient field-emission cathode material.These excellent properties make NdB_6 nanomaterials promising materials for use in vacuum electronic devices [12]. Thus, NdB_6 is antiferromagnetical at TN = 7.74 K[13]. Ding et al.[14] successfully synthesized NdB_6 Nanowires(NWs) by a self-catalyst method. Nanowires with diameters of approximately 80 nm and lengths spanning several micrometers have monocrystalline structures. Xu et al.[15] successfully produced NdB_6 nanostructures using a free-CVD process. The NdB_6 nanostructures exhibited a good stability. The effect of temperature on NdB_6 is important. When the temperature was increased, the turn-on and threshold electric fields decreased. The work function of NdB_6 nanostructures is considerably decreased as the temperature increases, leading to much enhanced field emission characteristics.

Tsuji et al. [16], studied the magnetoresistance, magnetization and specific heat of $Nd_xLa_{1-x}B_6$ (x=0. 9, 0.8, 0.7, 0) by a FZM method. The magnetoresistance, magnetization and specific heat are affected by temperature. As the temperature increased the others increase. Chaolong et al.[17] succesfully investigated $Nd_xLa_{1-x}B_6$ bulks using Spark Plasma Sintering (SPS) method. The work function of $Nd_xLa_{1-x}B_6$ was 2.72 eV. The Nd content enhanced thermionic emission characteristic and decreased the work function.

Li et al.[18] fabricated successfully high-quality, uniform $La_xNd_{1-x}B_6$ nanowires by catalyst-free CVD technique. $La_xNd_{1-x}B_6$ nanowires exhibit a superb field emission performance. Nanowires are used in optoelectronic devices such as nanoelectronic building blocks and flat panel displays.

Ab initio material modelling based on DFT was performed Quantum Espresso software (QE) packages based on modelling the material at nanoscales or on an atomic scale [19]. First- principles calculations were performed using the VASP [20]. The Projector Augmented Wave (PAW) method and the functional form of the Generalized Gradient Approximation(GGA) of Perdew–Burke–Ernzerhof (PBE) were preferred for exchange. The kinetic energy cut-off of the plane-wave basis set was 500 Ry. The Brillouin zone integration was performed at 3 × 3 × 3 k mesh points using methfessel-paxton smearing with a width of 0.02 Ry. A k-mesh 3 × 3 × 3 was used in the brillouin zone integration with Methfessel-Paxton smearing width of 0.02 Ry. Both LaB_6 and NdB_6 have cubic CsCl-type structures with a space group of Pm-3m symmetry [21].

RESULTS AND DISCUSSION

The bulk unit cell of REB_6 is simple cubic and is found in the symmetry of the space group Pm3̄m. The lattice of NdB_6 can be entirely defined using merely the lattice constant, a, and the positional parameter, z, as indicated in Figure 1. The lattice constant, was 1, intra-octahedral boron bond was 2, and inter-octahedral boron bond was 3.

Figure 1. NdB_6 structure showing relevant bond lengths.

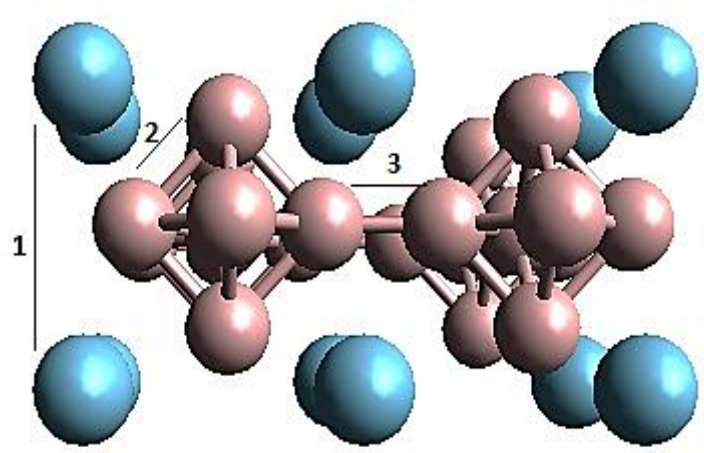

Table 1. The lattice constant (1), intra-octahedral boron bond (2), inter-octahedral boron bond (3), and positional parameter (z) of REB_6. z=3/2*1

		1 (Å)	2 (Å)	3 (Å)	z (Å)
LaB_6	Present study	4.157	1.766	1.66	0.226
	Previous results	4.154[5],4.15[9],4.156[22],4.145[23],4.156[24], 4.155[25],4.155[26], 4.151[8],4.15[8][27],4.176[28]	1.766[29],	1.659[29]	
$La_7Nd_1B_6$	Present results	4.267	1.857	1.801	0.227
	Previous results				
$La_1Nd_7B_6$	Present results	4.449	1.812	1.801	0.223
	Previous results				
NdB_6	Present results	4.118	1.75	1.643	0.227
	Previous results	4.125[30],4.132[11], 4,12[31], 4.1 [15],4.157[28], 4.126[32], 4.128[33]			

Table 1 lists the positional parameters of the given REB_6. The lattice constant of LaB_6 (Pm-3m space group) was calculated as a value of 4.157 Å. This was consistent with the experimental consequences indicated in Table 1. Furthermore, parameters 2 and 3 were 1.766 and 1.660 Å, respectively, with a boron positional parameter of approximately z=0.226 Å. Chen et al. [29] conducted a study on the structural refinement and thermal expansion of hexaborides. In this study, based on the X-ray powder diffraction technique, the intra-octahedral and inter-octahedral boron–boron distances were calculated as 1.766 and 1.659 Å, respectively. Xiao et al. investigated the optical features of LaB_6 using first-principles DFT calculations. They calculated the LaB_6 parameter to be 4.154 Å[34]. Hasan et al.[35] synthesized LaB_6 *via* carbothermal reduction. The calculated value of the lattice parameter was 4.157 Å. Furthermore, other experimental studies [36], [37] are consistent with those of presidential study. Mackinnon et al.[38] calculated the lattice constant of LaB_6 using DFT calculations. The calculated boron parameter (z) was 0.225 Å.

The doping of Nd instead of one La atom led to a slight increase in the lattice constant to 0.502 Å. In addition, 2 and 3 parameters were found to be 1.857 and 1.801 Å, respectively, which indicates an increase in these parameters while the z parameter remains nearly the same as that of LaB_6. In a study related to $LaxGd_{1-x}Bd_6$

synthesized by the SPS technique, the doping of Gd into LaB_6 strengthened the lattice parameters of the structure [39]. In a similar study, Chao et al. [40] fabricated $La_7Sm_1B_6$ by solid-state technique. Sm doping led to a decrease in the $La_7Sm_1B_6$ lattice.

The 1,2,3 and z parameters;1 of $La_1Nd_7B_6$ were found as 4.449, 1.812, 1.801, and 0.223 Å respectively. Compared to LaB_6, the ratio of Nd/La increased in parameters 1 2, and 3 but the parameter z didn't change considerably. On the other hand, Li et al. [18] conducted a study of single-crystal $La_xNd_{1-x}B_6$ nanowires to investigate the field emission performance and characterization. In this study, when Nd-doped into LaB_6, the lattice parameter of $La_xNd_{1-x}B_6$ was decreased. In a similar study, Chao et al. [40] produced $La_xSm_{1-x}B_6$ by solid-state reaction. They employed DFT to describe the characteristic of Sm-doped LaB_6. They obtained the lattice parameters of $La_{0.2}Sm_{0.8}B_6$ and $La_{0.4}Sm_{0.6}B_6$ as 4.123 and 4.128, respectively. Their results showed that doping LaB_6 with Sm decreases the lattice parameter of $La_xSm_{1-x}B_6$. When the La content was doped into BaB_6, the calculated value of the lattice constant of $La_1Ba_7B_6$ was increased [41]. Luo et al.[42] studied $La_1Ca_7B_6$ by first-principles calculations. Ca doping provides increases in the lattice strength of $La_1Ca_7B_6$.

The lattice constant of NdB_6 was calculated as a value of 4.118. Ali et al.[13] studied the thermoelectric power of NdB_6 by using the floating zone method. They measured the lattice constant was 4.126 Å. In other studies, Ping et al. [43] conducted a study of NdB_6 by using the first principle method. The lattice parameter of NdB_6 was calculated as 4.069Å. Sandeep et al. [36] calculated the lattice parameter of NdB_6 (4.157 Å) using the Full-Potential Linearized Augmented Plane Wave (FP-LAPW) technique. Furthermore, parameters 2 and 3 were found to be 1.750 and 1.643 Å, respectively, and the z parameter was 1.643 Å. Mackinnon et al.[38] determined the z parameter as 0,226 Å.

Figure 2 illustrated PDOS of $La_xNd_{8-x}B_6$ (x=0,1,7,8). As explicated in Figures 2(A) and 2(C) PDOS curves. La d-electron bands show typical conductive behavior as they pass fermi energy. The lowermost Conduction Bands (CBs) consisted of B s and the uppermost Valence Bands (VBs) have consisted of B p are indicated in Figure 2(B). La d-electron band passing Fermi energies are shown in Figure 2(C). The calculation converged with great intensity to a metallic ground state at the EF, at the Fermi level, as shown in the figure. The zone near EF is contributed mostly by La d states as explicit in Figures 2(B) and 2(C). Besides that, EF is contributed generally by Nd d states as shown in Figures 2(E) and 2(G). This is obvious that the energy division of the La d states and Nd d states additives look alike to B 2p additives, which is a signature of hybridization between La d-Nd d - B 2p states.

Figure 2. The Partial Density of States (PDOS) of A) LaB_6 B) B of LaB_6 C) $La_7Nd_1B_6$ D) B of $La_7Nd_1B_6$ E) $La_1Nd_7B_6$ F) B of $La_1Nd_7B_6$ G) NdB_6 H) B of NdB_6.

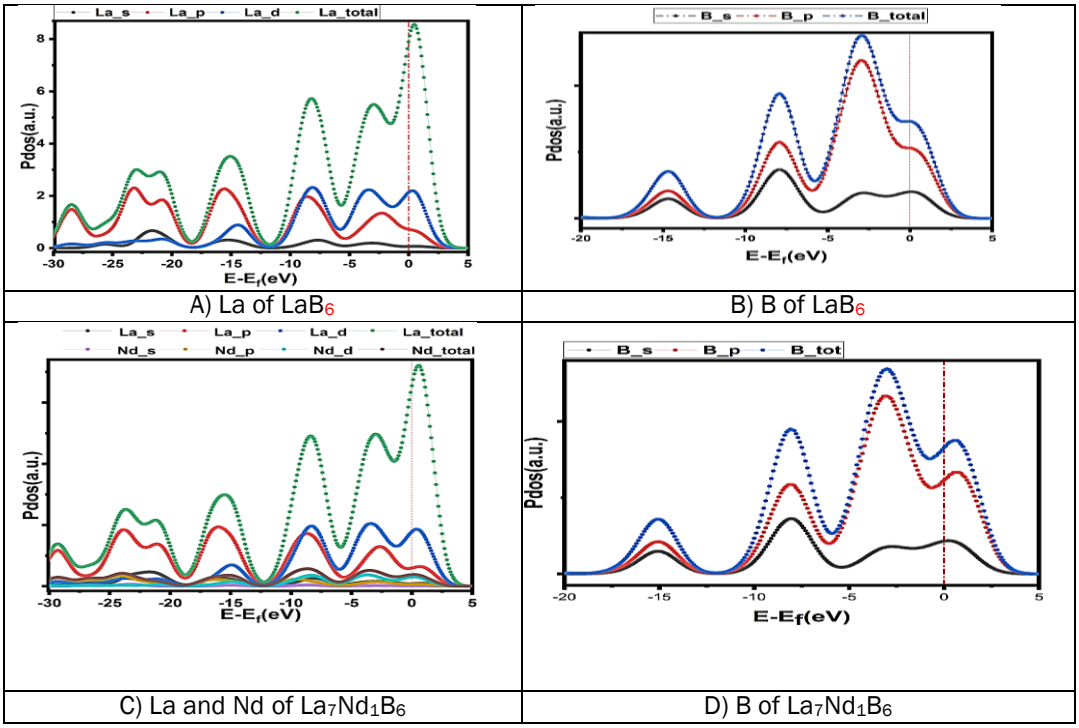

A) La of LaB_6 | B) B of LaB_6

C) La and Nd of $La_7Nd_1B_6$ | D) B of $La_7Nd_1B_6$

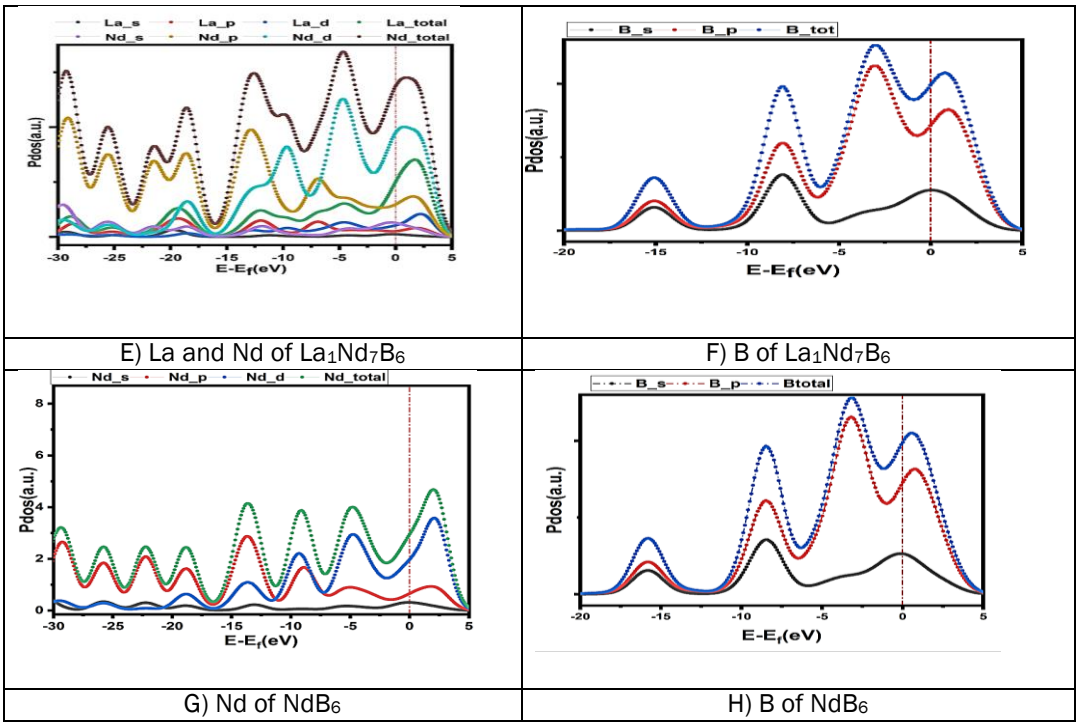

E) La and Nd of $La_1Nd_7B_6$ | F) B of $La_1Nd_7B_6$

G) Nd of NdB_6 | H) B of NdB_6

Figure 3 shows the charge density of LaB_6, $La_7Nd_1B_6$, $La_1Nd_7B_6$ and NdB_6. Light and dark colours show high and low- intensity zones respectively. Dark and light colours indicate low and high-density regions, respectively. $La_1Nd_7B_6$ has a low-density region and LaB_6 has a high-density region. There are six boron atoms on the plane. The centre of the figure was seen the strong B-B bonds. The LaB_6 midpoint has strong charge density peaks. $La_1Nd_7B_6$ has weak peaks.

Figure 3. The charge density of A) LaB_6 B) $La_7Nd_1B_6$ C) $La_1Nd_7B_6$ D) NdB_6.

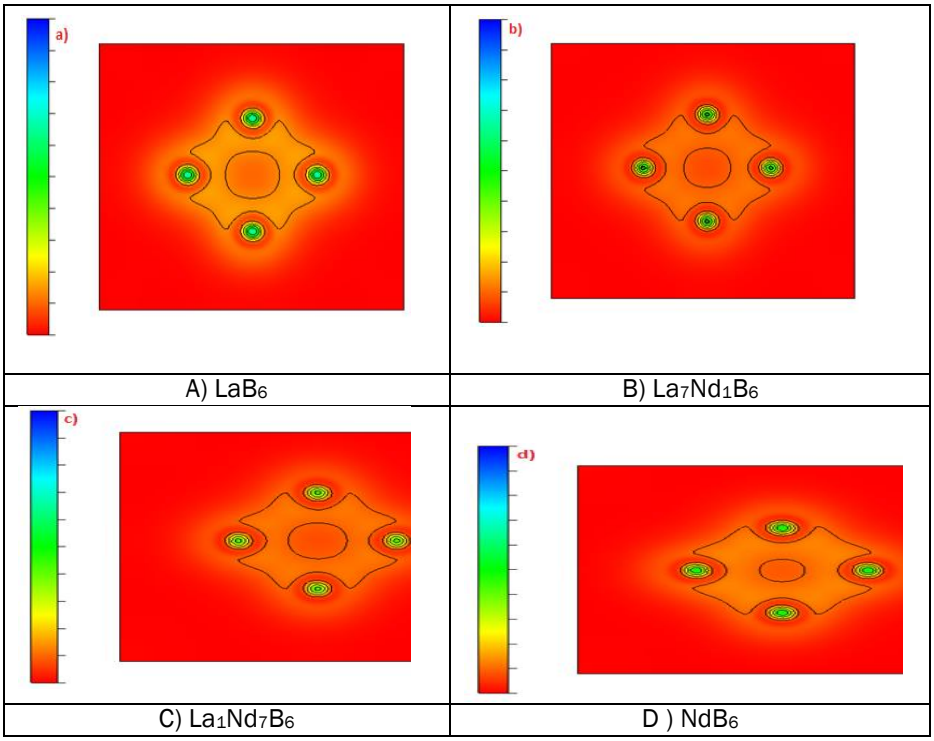

A) LaB_6 | B) $La_7Nd_1B_6$

C) $La_1Nd_7B_6$ | D) NdB_6

CONCLUSION

We comprehensively studied the mechanical and electronic properties of LaB_6, NdB_6, Nd-doped LaB_6 and La-doped NdB_6 using the density functional theory. The lattice constant of LaB_6 was lower than that of Nd-doped LaB_6. In addition, La doping increased the lattice constant of La-doped NdB_6. We calculated the PDOS of LaB_6, B for LaB_6, $La_7Nd_1B_6$, B for $La_7Nd_1B_6$, $La_1Nd_7B_6$, B of $La_1Nd_7B_6$, NdB_6, and B of NdB_6. We found that the La d-electron bands pass the Fermi energy. The light color in the charge density indicates that LaB_6 has a high-density region. Similarly, dark colour in the charge density shows that. $La_1Nd_7B_6$ has a low-density region.

REFERENCES

1. Zeng X, et al. First-principles study of the nonlinear elasticity of rare-earth hexaborides REB_6 (RE = La, Ce). Crystals. 2017;7:320.
2. Ji XH, et al. Rare-earth hexaborides nanostructures: recent advances in materials, characterization and investigations of physical properties. Prog Solid State Chem. 2011;39:51-69.
3. Liu H, et al. The electronic structures and work functions of (100) surface of typical binary and doped REB6 single crystals. Appl Surf Sci. 2018;434:613–619.
4. Zeng X, et al. First-principles study of the nonlinear elasticity of rare-earth hexaborides REB_6 (RE= La, Ce). Crystals. 2017;7:320.
5. Liu H, et al. The electronic structure and work functions of single crystal LaB_6 typical crystal surfaces. Vacuum. 2017;143: 245–250.
6. Uijttewaal MA, et al. Ab initio and work function and surface energy anisotropy of LaB_6. J Phys Chem B. 2006; 110:18459–18465.
7. Yu Y, et al. Synthesis of single-crystalline lanthanum hexaboride nanocubes by a low temperature molten salt method. Mater Chem Phys. 2018;207:325-329.
8. Zhang M, et al. A low-temperature route for the synthesis of nanocrystalline LaB_6. J Solid State Chem. 2008; 181:294-297.
9. Yu Y, et al. Low temperature synthesis of LaB_6nanoparticles by a molten salt route. Powder Technol. 2018; 323:203-207.
10. Dou HZ, et al. A new method of preparing NdB_6 ultra-fine powders. Rare Met. 2015:1-7.
11. Yadav KK, et al. Excellent field emission from ultrafine vertically aligned nanorods of NdB6 on silicon substrate. Appl Surf Sci. 2020; 526:146652.
12. Wang G, et al. Morphological evolution of neodymium boride nanostructure growth by chemical vapor deposition. J Phys Chem C. 2009;113:10446-10451.
13. Ali N. Low temperature thermoelectric power of LaB_6, PrB_6 and NdB_6. Solid State Commun. 1983;46:33-35.
14. Ding Q, et al. Large-scale synthesis of neodymium hexaboride nanowires by self-catalyst. Solid State Commun. 2007;141:53-56.
15. Xu J, et al. Excellent Field-Emission Performances of Neodymium Hexaboride (NdB_6) Nanoneedles with Ultra-Low Work Functions. Adv Funct Mater. 2013;23:5038-5048.
16. Tsuji S, et al. Rapid Suppression of the Metamagnetic Transition for H||‹ 111› in NdB_6 by La Doping. J Phys Soc Japan. 2002;71:2994-3002.
17. Chao-Long L, et al. Preparation and property of $La_{1-x}Nd_xB_6$ cathode material. J Inorg Mater. 2015; 30:363-368.
18. Li Q, et al. Single-crystalline La_x $Nd_{1-x}B_6$ nanowires: synthesis, characterization and field emission performance. J Mater Chem C. 2015; 3:7476-7482.
19. Giannozzi P, et al. Advanced capabilities for materials modelling with Quantum ESPRESSO. J Phys Condens matter. 2017;29:465901.
20. Hobbs D, et al. Fully unconstrained noncollinear magnetism within the projector augmented-wave method. Phys Rev B. 2000; 62:11556.
21. Hacker H Jr, et al. Magnetic susceptibility of neodymium hexaboride. Solid State Commun. 1968; 6:379-381.
22. Tekoğlu E, et al. Characterization of LaB_6 particulate-reinforced eutectic Al-12.6 wt% Si composites fabricated *via* mechanical alloying and spark plasma sintering. Powder Technol. 2018;340:473-483.
23. Xiao Y, et al. Single-crystal LaB_6 field emission array is rapidly fabricated by ultraviolet femtosecond laser and its field electronic structure characteristics. Vacuum. 2021;184:109987.
24. Soloviova TO, et al. Thermal dependent properties of LaB_6-MeB_2 eutectic composites. Ceram Int. 2021;47: 17667-17677.
25. Ivashchenko VI, et al. Electronic, thermodynamics and mechanical properties of LaB6 from first-principles. Phys B Condens Matter. 2018;531:216-222.

26. Otani S, et al. Preparation of LaB_6 single crystals from a boron-rich molten zone by the floating zone method. J Cryst Growth. 1993;126: 466–470.
27. Bai L, et al. Structure and chemical bond characteristics of LaB_6. Phys B Condens Matter. 2009;404: 4086-4089.
28. Ghimire MP, et al. Study of Bulk modulus, Volume, Energy, lattice parameters and magnetic moments in rare earth hexaborides using density functional theory. J Phys Conf Ser. 2012;377:12084. [Google scholar]
29. Chen C-H, et al. Structural refinement and thermal expansion of hexaborides. J Alloys Compd. 2004;366:L6–L8.
30. Simsek T, et al. Nano-sized neodymium hexaboride: Room temperature mechanochemical synthesis. Phys B Condens Matter. 2019;570:217-223.
31. Han W, et al. Synthesis of single-crystalline NdB_6 submicroawls via a simple flux-controlled self-catalyzed method. RSC Adv. 2015; 5:12605-12612.
32. Blomberg MK, et al. Single-crystal X-ray diffraction study of NdB_6, EuB_6 and YbB_6. J Alloys Compd. 1995;217:123-127.
33. Qinghua F, et al. Field emission from one-dimensional single-crystalline NdB_6 nanowires. J Rare Earths. 2013; 31:145-148.
34. Xiao L, et al. Origins of high visible light transparency and solar heat-shielding performance in LaB_6. Appl Phys Lett. 2012;10:41913.
35. Hasan M, et al. Low temperature carbothermal and boron carbide reduction synthesis of LaB_6. J Alloys Compd. 2013;578:176-182.
36. Sandeep MP, et al. Study of Bulk modulus, Volume, Energy, lattice parameters and magnetic moments in rare earth hexaborides using density functional theory. J Phys Conf Ser 2012;377:12084.
37. Hasegawa A, et al. Energy bandstructure and Fermi surface of LaB_6 by a self-consistent APW method. J Phys F Met Phys. 1977;7:1245.
38. Mackinnon I, et al. Metal hexaborides with Sc, Ti or Mn. Model Numer Simul Mater Sci. 2013;3:158-169.
39. Bao LH, et al. In situ (La_xGd_{1-x}) B_6 cathode materials prepared by the spark plasma sintering technique. Phys Scr. 2012;85:35710.
40. Chao L, et al. The effect of Sm-doping on optical properties of LaB_6 nanoparticles. J Alloys Compd. 2015;622:618–621.
41. Hasan MM, et al. Low temperature synthesis of low thermionic work function (La_xBa_{1-x}) B_6. J Alloys Compd. 2015;636: 67-72.
42. Luo K, et al. Crystal structures and mechanical properties of M (Mg, Sr, Ba, La) $_xCa_{1-x}B_6$ solid solution: A first principles study. Ceram Int. 2016;42:6632-6639.
43. Qin P, et al. Electronic and Optical Properties of RB_6 (R= La, Nd): A Computer Aided Design. Adv Mat Res. 2012;571:239-242.